AIAA SciTech Forum
23-27 January 2023, National Harbor, MD & Online
AIAA SCITECH 2023 Forum

10.2514/6.2023-2183

Design of Pre-Combustion Chambers for Hybrid Propellant Rocket Motors and Related Aspects

Maurício S. Gontijo*, Renato B. N. Filho†
Aeronautics Institute of Technology, São José dos Campos, São Paulo, 12228-900, Brazil

Caio H. F. L. Domingos‡
Akaer, São José dos Campos, São Paulo, 12247-014, Brazil

Hybrid Propellant Rocket Motors (HPRM) are advancing fast technologically in the last few years. These improvements are finally increasing its competitiveness in the launch market around the world. But yet, some topics still requires more deep studies, such as the pre-chamber design. A low amount of literature references explore deeply this subject. This work proposes a low computational cost algorithm that predicts the minimum pre-chamber length with a vaporization model and through a feed-system coupled instability model. This type of analysis is a key tool to minimize the rocket weight, size and losses. In addition, it can be coupled with internal ballistics codes. Furthermore, a comparison of the results were made with real hybrid motors to guarantee reliability of the results. This comparison allowed to propose a range of L_{pc}/d_{pc} from 0.26 to 0.66 in order to have complete vaporization.

I. Nomenclature

A	=	area
C_D, C^*, C_c	=	discharge coefficient, characteristic velocity and contraction coefficient
c	=	characteristic dimension
c_p	=	specific heat at constant pressure
c'	=	boundary-layer delay time coefficient
D	=	mass diffusivity
d	=	diameter
h	=	heat transfer coefficient
K, K_c	=	mass transfer coefficient and cavitation weighting parameter
k	=	thermal conductivity
L	=	length
M	=	molecular weight
$\dot{m}$	=	mass flow rate
Nu	=	Nusselt number
n	=	number of moles
Oh	=	Weber number
P	=	pressure
Pr	=	Prandtl number
q	=	heat
Re	=	Reynolds number
R, R_u	=	specific and universal gas constant
r, r_{in}	=	radius and radius of the orifice inlet fillet
S	=	drag coefficient
Sc, Sh, SMD	=	Schmidt number, Shearwood number and Sauter Mean Diameter
T	=	temperature

*Masters student, Aerospace Propulsion and Energy - Aeronautics Institute of Technology, mauricio.sa.gontijo@gmail.com.
†Masters student, Aerospace Propulsion and Energy - Aeronautics Institute of Technology, renatobnf@gmail.com.
‡MSc Aerospace Engineer, Systems engineering, caiohf8@gmail.com.

t, t_f	=	time and gas film thickness
V	=	volume
v	=	velocity
We	=	Weber number
Z	=	term for the account of the sensible heat
z	=	exponent of the Z term
$\alpha\alpha_d$	=	growth in oscillation amplitude and correction factor for uni-directional mass transfer
β	=	ratio of average chamber pressure by twice the pressure drop
ϕ	=	equivalence ratio
λ	=	latent heat of vaporization oft the droplet
κ	=	weighting factor
μ, ν	=	dynamic and kinematic viscosity
ρ	=	density
$\mathcal{T}$	=	relation of residence times
τ	=	residence time

Upperscripts

*	=	characteristic parameter

Subscripts

c	=	chamber related
d	=	droplet related
ex	=	experimental parameter
f	=	fuel related
g	=	gas related
i	=	injector orifice related
L	=	liquid phase related
ox	=	oxidizer related
m	=	mean vapor-gas mixture related
p	=	grain port related
pc	=	pre-combustion chamber, or pre-chamber, related
r	=	related to a whole process (e.g., injection, atomization, mixing and combustion)
t	=	nozzle throat related
th	=	theoretical parameter
v	=	vapor phase related
$1, 2$	=	upstream property (e.g., tank or manifold) and downstream property (e.g., combustion chamber)

II. Introduction

In hybrid propulsion, generally, a liquid oxidizer is injected inside the combustion chamber to react with a solid fuel. In order to combust, the oxidizer has to vaporize and the fuel has to liquefy and vaporize. These characteristics, allied with low regression rates, in comparison with solids, make the combustion chambers of hybrid motors relatively large, mainly in comparison with liquid propellant rocket engines. This disadvantage is one of the most impacting point that prevents hybrid rockets to be more competitive in the market, even though it is a promising technology [1–3].

The components responsible to provide enough residence time for the oxidizer and the fuel are the pre and post-combustion chambers, respectively. The pre-chamber grants that the oxidizer is fully injected, atomized and vaporized. In case the pre-chamber is too small, combustion instabilities and nonuniform burn of the grain may appear. On the other hand, if it is too large, heat transfer losses and an increase in weight become significantly high [1, 4–6].

A. Overview of Methods for Rocket Chamber Design

In general, literature provides only empirical relations to calculate the pre-combustion chamber length (L_{pc}) and some researches designs it numerically, with the aid of CFD (Computational Fluid Dynamics) softwares [7]. [1] recommends, as a rule of thumb, that the pre-chamber L/D is about 0.5, also used in [8]. [4, 5] presents a model that results in a pre-chamber length required to suppress feed-system coupled combustion instabilities. However, in order to decrease computational costs, in comparison with CFD, and increase accuracy, in comparison with empirical relations, a vaporization model could be employed with the objective of predicting the L_{pc}. In this type of application, the length required for the droplets breakups can be neglected due to the Reynolds, Ohnesorge and Weber numbers usually obtained [9]. Therefore, a reasonable L_{pc} is the length for complete vaporization.

Vaporization models are widely employed in liquid propulsion systems [10]. In [11] it is presented two simple models, one with no combustion and other with combustion. In addition, a third (and more accurate) model is shown, which is a one-dimensional vaporization-controlled combustion model. In [12–16], it is shown a one-dimensional model capable of even predicting the characteristic velocity (C^*) efficiency based on percentage of vaporized propellant at the end of the chamber. The works [17–19] presents a one-dimensional vaporization model capable of calculating the characteristic length (L^*), considering even the chemical reaction rate. Other works presented some additional contributions, such as turbulence intensity influence [20, 21], droplets thermal expansion and deformation due to drag [22], vaporization of a group of droplets, sub-critical vaporization and others [23]. The works published by [24–26] validates the model presented by [12–16] with interesting discussions and added a empirical correlation to calculate the length to vaporize 95% of the propellant. In addition, the works [27–29] discussed more deeply some parameters of the model presented by [17–19], presented validations in comparison with more real engines and with various propellant mixtures and proposed a new propulsive parameter important for the L^*, the ϕ^*. ϕ^* is called characteristic equivalence ratio and it is defined as the equivalence ratio (ϕ) required to reach the minimum L^* for a given chamber pressure and propellant mixture. Also, those last three works came with the same conclusions in comparison with [24–26], that the droplet size is the main parameter that controls the chamber length, and in order to decrease the required length, the droplets size, injection velocity, final gas velocity and contraction ratio must decrease and chamber pressure and initial droplet temperature must increase. All of these models and other discussions are presented in [10].

While many works make use of vaporization models on liquid propulsion, there is a lack of studies in this field in hybrids. This work intends to implement an algorithm, based on [12–16], to analyze and design pre-combustion chambers of HPRMs with liquid oxidizers. Besides that, other factors influencing the design of the pre-chamber are discussed. Additionally, the results were obtained for a nitrous oxide (N_2O), or dinitrogen monoxide, since it is one of the most used used oxidizers in hybrid propulsion and a validation was made with motors that uses this oxidizer.

N_2O is used mostly due to be storable, self-pressurizing, green, nontoxic, etc. However, it has some disadvantages such as lower specific impulse, in comparison with Liquid Oxygen (LOx), two-phase flow, low critical point, etc [30].

III. Injection System

A. Aspects of Design

One of the main parameters while designing the injection system is the Sauter Mean Diameter (SMD or also known as D_{32}), which is a measurement of the ratio of the volume to the surface area of the spray (the mass mean diameter also are commonly used, but it is around 15% to 25% larger than the SMD) [31]. Also, the environment is an atmosphere rich in oxidizer with lower temperature than the adiabatic flame temperature, since there is no fuel (then, no combustion) in the pre-chamber.

The equation below presents the SMD model used for the showerhead injector (plain-orifice atomizer), and its variation with the injector pressure drop is shown in Fig. 1b, which is from Merrington and Richardson's experiments [31]:

$$\mathrm{SMD} = \frac{500 d_i^{1.2} \nu_L{}^{0.2}}{v_i} \tag{1}$$

where d_i is the orifice diameter, ν_L is the liquid kinematic viscosity and v_i is the injection velocity, which is defined below for an incompressible fluid through the continuity equation:

$$v_i = \sqrt{\frac{2\Delta P}{\rho_L}} = \sqrt{\frac{2P_2 - P_1}{\rho_L}} \tag{2}$$

where the subscripts 1 and 2 are for upstream and downstream, respectively, ρ_L is the liquid density and ΔP is the pressure drop along the injector orifice, in general around 20% of the chamber pressure. Additionally, there are three main dimensionless parameters that describes the behavior of the injected fluid. Oh is the Ohnesorge number, which compares the viscosity influence with the injected droplet deformation forces. Another two important parameters that characterizes the breakup process are the Reynolds number (Re), which compares the inertia force with the viscous force, and the Weber (We), which compares the inertia force to the surface tension force [9, 23, 31–33]. Those non-dimensional numbers are related by the following relation and graph:

$$\mathrm{We} = (\mathrm{OhRe})^2 \begin{cases} \mathrm{Re} = \dfrac{\rho v_i c}{\mu} \\ \mathrm{Oh} = \dfrac{\mu}{\sqrt{\rho \sigma d_i}} \\ \mathrm{We} = \dfrac{\mu {v_i}^2 d_i}{\sigma} \end{cases} \tag{3}$$

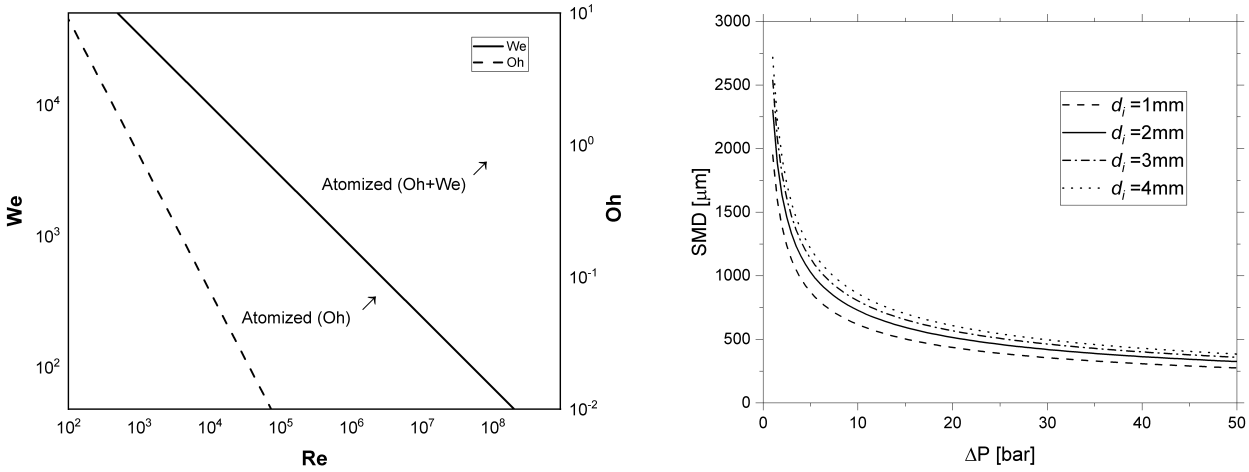

(a) (b)

Fig. 1 (a) SMD in function of ΔP for constant $\rho_L = 1011.2$kg/m³ and $\nu_L = 1.2332 \cdot 10^{-07}$m²/s, (b) Atomization transition regions of the injected propellant in function of We**,** Re **and** Oh**, adapted from [34].**

where ρ, μ and σ are the fluid density, dynamic viscosity and surface tension, respectively, c is the characteristic dimension (in case of an injector orifice, $c = d_i$). The great majority of rocket injectors are located in the atomized regions shown in Fig. 1a, this is the reason that no breakup processes (that may occur before the atomization) are being discussed in this work.

The discharge coefficient is the ratio between the theoretical and experimental mass flow rates. In case of oxidizers such as N_2O, the flow inside the injector is under cavitating condition [31]. This means that the discharge coefficient (C_D) is related only to cavitation number. In case of non-cavitating oxidizers, such as LOx, its vapor pressure is low [35] and the cavitating number tends to zero, then the C_D is calculated through [31]:

$$C_D = \frac{\dot{m}_{th}}{\dot{m}_{ex}} = \left[1.23 + \frac{58\,(L_i/d_i)}{\mathrm{Re}}\right]^{-1} \tag{4}$$

where $\dot{m}_{th}$ and $\dot{m}_{ex}$ are the theoretical and experimental mass flow rates, respectively, and L_i is the orifice length. The equation above is valid for the range of L_i/d_i from 2 to 5 and Re from 100 to $1.5{\cdot}10^5$.

B. Aspects of Two-Phase Oxidizers Injection

In case of cavitation condition, C_D is defined as:

$$C_D = C_C \cdot \sqrt{K_c} = \left[\left(\frac{1}{0.62}\right)^2 - \frac{11.4 r_{in}}{d_i}\right]^{-0.5} \cdot \sqrt{\frac{p_1 - p_v}{p_1 - p_2}} \tag{5}$$

where p_1, p_2 and p_v are the upstream, downstream and vapor pressures, respectively, and r_{in} is the radius of the orifice inlet fillet. Also, K_c is a cavitation weighting parameter and C_C is a contraction coefficient [36]. The equation for C_C works for sharp-edge and rounded injector orifice inlet. In addition, it works only for $0 \leq r_{in}/d_i \leq 0.14$, since higher values of r_{in}/d_i will not form a vena contracta.

Although many of the equations presented in this section are focused in a showerhead configuration, similar relations exists for other types of injectors and the following sections are also applied for them.

Another disclaimer is that, since N_2O is a two-phase oxidizer under saturation condition (at ambient temperature), a model for predicting the propellant mass flow rate accurately should be used. One of the most used tank emptying models is the one proposed by [37], based on the two-phase model proposed by [38]. Some years later, a correction was made on Whitmore and Chandler's model by [39]. This model is known to be the Nonhomogeneous Nonequilibrium (NHNE) model, which is a weighting between the Homogeneous Equilibrium Model (HEM) and the Single Phase Incompressible (SPI) model based on the ratio of the characteristic bubble growth time (τ_b) and the residence time of the liquid in the injector element (τ_i). The following relations describe briefly this model:

$$\text{NHNE}: \ \dot{m}_{NHNE} = \frac{\kappa \cdot \dot{m}_{SPI}}{1+\kappa} + \frac{\dot{m}_{HEM}}{1+\kappa} \begin{cases} \dot{m}_{SPI} = C_d \sqrt{2\rho_1 (\Delta P)} \ ; \ \text{SPI} \\ \dot{m}_{HEM} = C_d \rho_2 \sqrt{2 (\Delta h)} \ ; \ \text{HEM} \\ \kappa = \dfrac{\tau_b}{\tau_i} = \sqrt{\dfrac{P_1 - P_2}{P_v - P_2}} \ ; \begin{cases} \tau_b = \sqrt{\dfrac{3\rho_L}{2(P_v - P_2)}} \\ \tau_i = L_i \sqrt{\dfrac{\rho_L}{2(P_1 - P_2)}} \end{cases} \end{cases} \tag{6}$$

where $\dot{m}_{NHNE}$, $\dot{m}_{SPI}$ and $\dot{m}_{HEM}$ are the NHNE, SPI and HEM mass flow rates, respectively, and κ is the weighting factor. All properties are evaluated under saturation condition in function of temperature, for upstream properties, and in function of pressure, for downstream properties and can be obtained at [40].

It is important to mention that are other tank emptying models available and all of them are described in [41] with their advantages and disadvantages, such as the ones proposed by [42]. Some discussions and analysis were made in order to understand the impact of each portion of mass flow rate, based on analytical calculations and experimental results, in [43–45]. In addition, [35] make relevant discussions about the physics of nitrous oxide and recent researches are improving two-phase models for hybrid propulsion, accounting for chocked mass flow conditions [46].

IV. Impact on Combustion Instability

A. Feed-System Coupled Instability

A certain dependence of the pre-chamber on the feed-system coupled instability was analyzed by [4–6]. The theory was developed as an adaptation of the Summerfield theory, or L^* theory, for liquid propellant rocket engines [47]. It is based on the mass conservation equation, but for the hybrid philosophy. In addition, this model was validated experimentally with two motors, from the University of Brasilia (SARA [48]: UnB; Brazil) and Free University of Brussels (ULBHRE [49]: ULB; Belgium), with various injector types. The critical case for no chamber pressure oscillation for hybrids is:

$$0.5\beta^{-1} = \mathcal{T} = \frac{\tau_{pc} + 0.5\tau_f}{\tau_r} \tag{7}$$

where τ_{pc}, τ_f and τ_r are the residence time on the pre-chamber, fuel grain and combustion chamber, respectively and defined in Eq. 9, β is defined as:

$$\beta = \frac{\overline{P}_c}{2\Delta P} \tag{8}$$

$$\begin{cases} \tau_{pc} = \dfrac{2L_{pc}}{v_i + v_p} \\ \tau_f = c' \dfrac{V_f P_c}{\left(2\dot{m}_{ox} + \dot{m}_f\right) R\overline{T}_p} \approx c' \dfrac{n}{\left(2\dot{m}_{ox} + \dot{m}_f\right)} \\ \tau_r = \dfrac{V_c C^*}{A_t R T_c} = \dfrac{L^* C^*}{R T_c} \end{cases} \tag{9}$$

where $\overline{P}_c$ is the average chamber pressure, $\overline{T}_p$ is the average temperature in the port, v_p is the velocity in the port, $\dot{m}_{ox}$ and $\dot{m}_f$ are the oxidizer and fuel mass flow rates, respectively, V_c and T_c are the chamber volume and temperature, respectively, L_{pc} is the pre-chamber length, R is the gas constant, V_f is the port volume $(A_p \cdot L_f)$, n is the number of moles in the gas and c' is a boundary-layer delay time coefficient, which also is a correction factor obtained experimentally. In general, c' is approximately 0.55 [50], but it may vary (e.g., 2.05 was used in [4]). Physically, τ_{pc} is the time for the whole oxidizer injection, atomization and vaporization process to occur, τ_f is the time necessary for the boundary-layer properties to adjust to any changes in the oxidizer flux ,similar to the boundary-layer lag, and τ_r is the time for the gases to flow through the entire combustion chamber. The following graph shows the stability criterion for HPRM, where α (best described at [4–6]) represents the growth in oscillation amplitude, schematically shown below:

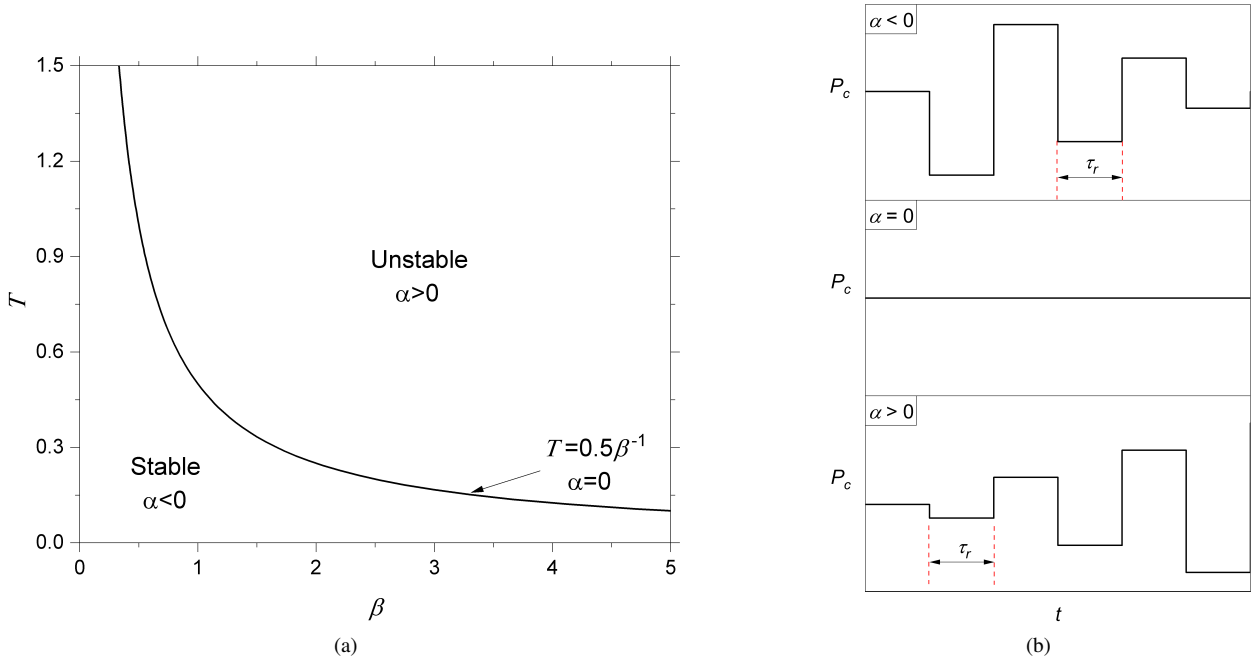

Fig. 2 (a) Stability criterion for HPRMs, adapted from [5], (b) Scheme of chamber pressure oscillations in function of α, adapated from [10].

As it is possible to analyze in Figs. 2a and 2b, the critical condition is when $\alpha = 0$, but if any perturbation is induced, it may increase the chamber pressure indefinitely. In addition, it is commonly assumed that a maximum 5% of oscillations means that the combustion is stable [3]. Eq. 7 is derived from the following relation [5], in which it is also possible to analyze the role of α:

$$\begin{cases} \alpha + {\tau_r}^{-1} = -\beta {\tau_r}^{-1} \left\{ e^{-\alpha \tau_{pc}} \cos\left(\tau_{pc}\, \omega\right) + e^{-\alpha\left(\tau_{pc} - \tau_f\right)} \cos\left[\left(\tau_{pc} - \tau_f\right) \omega\right] \right\} \\ \omega = \beta {\tau_r}^{-1} \left\{ e^{-\alpha \tau_{pc}} \sin\left(\tau_{pc}\, \omega\right) + e^{-\alpha\left(\tau_{pc} - \tau_f\right)} \sin\left[\left(\tau_{pc} - \tau_f\right) \omega\right] \right\} \end{cases} \tag{10}$$

B. Pre-Chamber Impact

In order to understand better how the pre-chamber impacts on the stability, a generic motor was evaluated. Assuming constant τ_f = 5ms, τ_r = 25ms, v_i = 70m/s and v_p = 0.24m/s, the following graph could be obtained:

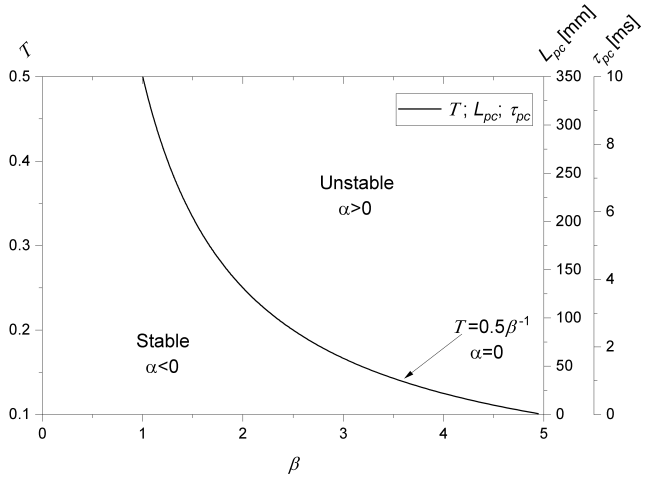

Fig. 3 Example of impact of L_{pc} and τ_{pc} on motor combustion instability.

Above, an example is shown how some design parameters impact directly on the motor's stability. With this example, a natural correlation between pre-chamber size and, consequently, the residence time with the combustion stability is observed.

A common way to avoid feed-system coupled instabilities is by using a cavitating venturi in the feed line. In this way, the combustion chamber is isolated from the feed system. However, using nitrous oxide is not recomended to implement a cavitating venturi, since it may suffer an explosive decomposition reaction. To overcome this issue, a choked injector is also capable of isolating the feed system [35].

V. Vaporization-Based Mathematical Model

The assumptions made on the mathematical model are listed below:

1) No combustion and chemical reactions, since there is no fuel in pre-chamber;
2) No breakup processes (atomized section of Fig. 1a);
3) Spherical droplets;
4) Constant thermophysical properties of the gas inside pre-chamber;
5) One-dimensional model;
6) Turbulence effects are neglected;
7) No droplets interactions;
8) Only convective heat transfer is considered;
9) Transient model in a steady state motor operation;
10) Use of liquid oxidizers;
11) Cavitating, choked flow in injectors is not being considered;
12) All droplets are injected with the same size, velocity and temperature.

In addition to the assumptions above, showerhead injectors are being taken in consideration in this work. However, other types of injectors are applicable to this theory.

The vaporization model is mainly ruled by the mass and energy conservation laws and by the interaction between the liquid of the droplet with the vapor film and the vapor film with the gas atmosphere. These interactions depends on thermophysical parameters and are ruled by the mass transfer, heat transfer, droplet heating rate, droplet acceleration and gas velocity equations [12–16, 24–26, 51]. This system of equation and how each equation acts on the droplet inside the pre-chamber are shown below:

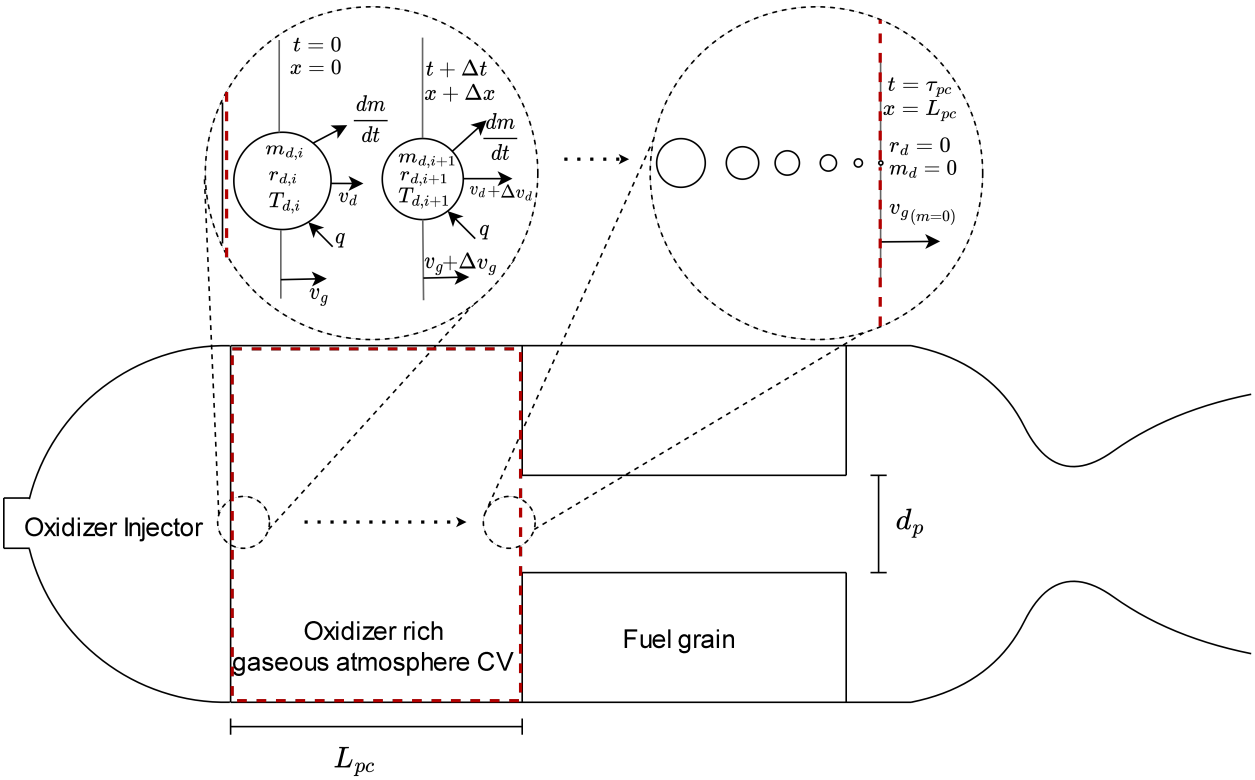

Fig. 4 Scheme of how each of governing equations acts on the vaporizing droplet inside a oxidizer rich gaseous atmosphere Control Volume (CV).

$$\begin{cases} \dfrac{dm}{dt} = A_d K \alpha_d P_d & ; \quad \text{Mass transfer} \\ q = hA_d \left(T_{pc} - T_d\right) Z & ; \quad \text{Heat transfer} \\ \dfrac{dT_d}{dt} = \dfrac{q - \dfrac{dm}{dt}\lambda}{mc_{p,L}} & ; \quad \text{Droplet heating rate} \\ \dfrac{dv_d}{dt} = -\dfrac{3Sv_{rel}{}^2\rho_m}{8r_d\rho_L} & ; \quad \text{Droplet acceleration} \\ v_g\left(x\right) = \dfrac{\dot{m}_{th}}{\rho_g \pi {r_p}^2}\left(1 - \dfrac{\dot{m}_{ox}\left(x\right)}{\dot{m}_{ox}\left(m=0\right)}\right) & ; \quad \text{Gas velocity} \end{cases} \tag{11}$$

where m is the droplet mass, A_d, P_d, T_d and r_d are the surface area, partial pressure, temperature and radius of the droplet (r_d = SMD/2), respectively, K is the mass transfer coefficient, h is the heat transfer coefficient, T_{pc} is the temperature inside pre-chamber, α_d is a correction factor for uni-directional mass transfer, Z is a term for the account of the sensible heat taken up by the diffusing vapor, λ is the latent heat of vaporization of the droplet at temperature T_d, $c_{p,L}$ is the specific heat at constant pressure of the droplet in liquid phase, v_d is the droplet velocity, v_{rel} is the relative velocity, ρ_m is the vapor-gas mixture density, v_g and ρ_g are the gas velocity and density, respectively, r_p is the grain port area and $\dot{m}_{ox}$ is the mass flow rate of vaporization of the oxidizer.

The mass transfer coefficient, K, is obtained below:

$$K = \frac{\mathrm{Sh} M_v D}{2 r_d R_u \overline{T}} \tag{12}$$

where M_v is the molecular weight of evaporating species, D is the coefficient of mass diffusivity, R_u is the universal gas constant (8.31446 J/(molK)), $\overline{T}$ is the mean temperature ($\overline{T} = (T_c + T_L)/2$) and Sh is the Shearwood number, which is calculated through Ranz Marshall relation [52]:

$$\mathrm{Sh} = 2 + 0.6 \sqrt[3]{\mathrm{Sc}} \sqrt{\mathrm{Re}} \tag{13}$$

where Sc is the Schmidt number, which is defined by:

$$\mathrm{Sc} = \frac{\mu_m}{\rho_m D} \tag{14}$$

where μ_m is the mean μ, which is calculated as shown in Eq. 18 (but for μ). The correction factor for uni-directional mass transfer is defined as:

$$\alpha_d = \frac{P_{pc}}{P_d} \ln \left(\frac{P_{pc}}{P_{pc} - P_d} \right) \tag{15}$$

The parameter Z is calculated through:

$$Z = \frac{z}{(e^z - 1)} \tag{16}$$

where z is calculated by:

$$z = \frac{\frac{dm}{dt} c_{p,L} t_f}{4\pi k_m r_d \left(r_d + t_f \right)} \tag{17}$$

where t_f is the gas film thickness and k_m is the mean value of thermal conductivity, calculated below:

$$k_m = \left(1 - \frac{P_d / P_{pc}}{2} \right) k_d + \frac{P_d / P_{pc}}{2} k_g \tag{18}$$

where k_d and k_g are the thermal conductivity of the droplet and gas, respectively. The heat transfer coefficient, h, is calculated through Ranz Marshall relation [52], but for Nusselt number (Eq. 20):

$$h = \frac{\mathrm{Nu} k_m}{d_d} \tag{19}$$

$$\mathrm{Nu} = 2 + 0.6 \sqrt[3]{\mathrm{Pr}} \sqrt{\mathrm{Re}} \tag{20}$$

where d_d is the droplet diameter(d_d = SMD) and Pr is the Prandtl number, which is calculated below:

$$\mathrm{Pr} = \frac{c_{p,m} \mu_m}{k_m} \tag{21}$$

where $c_{p,m}$ is the mean c_p, which is calculated as shown in Eq. 18 (but for c_p).

The droplet acceleration is derived from the Stokes drag law for a spherical object and the drag coefficient S is calculated through [53]:

$$S = 27 \mathrm{Re}^{-0.84} \tag{22}$$

The above equation was derived for Re from 6 to 400, but [12] tested it successfully for propellant droplets for numbers until 2000. In addition, other equations for S exists, such as the one presented by [54].

The vapor-gas mixture density ρ_{vg} is calculated through:

$$\rho_{vg} = \frac{P_c \overline{M}}{R_u T_m} \tag{23}$$

where $\overline{M}$ and T_m are the average molecular weight between vaporizing droplet and gas and it is calculated through:

$$\overline{M} = \left(1 - \frac{P_d/P_{pc}}{2}\right) M_d + \frac{P_d/P_{pc}}{2} M_g \tag{24}$$

where M_d and M_g are the molecular weight of the droplet and gas, respectively.

To solve the governing equations, a fourth order Runge-Kutta numerical method is used. In addition, the gaseous and liquid properties of the oxidizer are obtained through fittings and interpolations from data available at the National Institute of Standards and Technology (NIST) [40].

A computational algorithm was built in order to calculate the whole process described in the previous section. The algorithm is represented by the following flowchart:

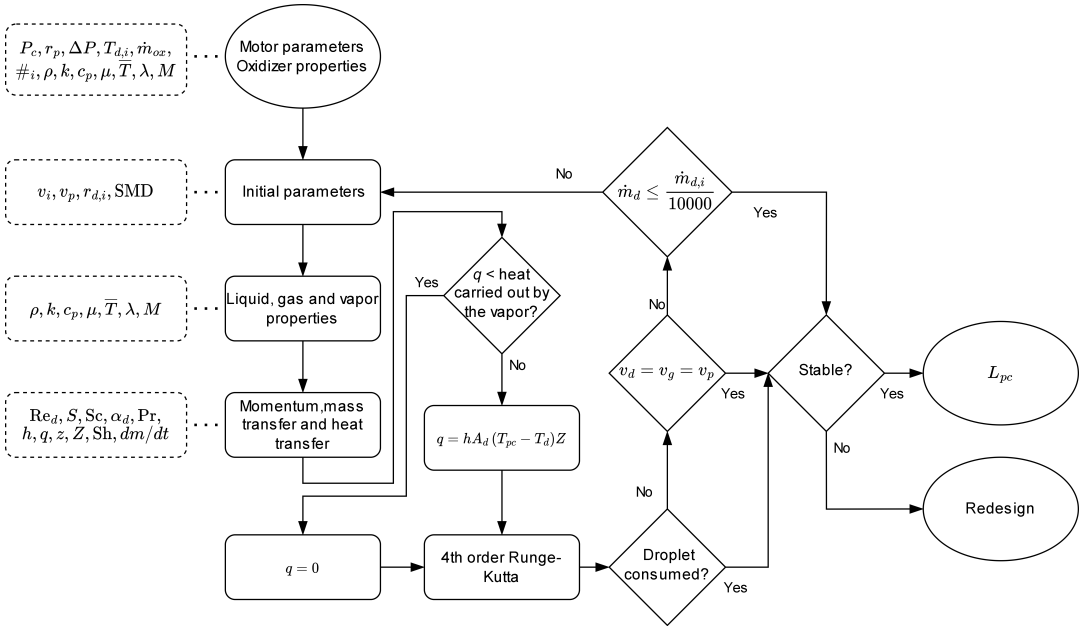

Fig. 5 Algorithm flowchart.

As it is seen above, there are three convergence criteria (by droplet consumption, mass transfer and gas and droplet velocity). In addition, if the system is stable, the pre-chamber is calculated. Otherwise, if it is not stable, the motor must be redesign.

VI. Results, Validation and Discussions

The algorithm reproduced test conditions presented at [4–6] and compiled in the table below:

Table 1 Parameters of the tested conditions

#	L_{pc}, mm	P_c, bar	ΔP, bar	$\dot{m}_{ox}$, kg/s	τ_{pc}, ms	τ_f, ms	τ_r, ms
1	56.6	25.2	24.7	0.211	7.5	6.1	26.7
2	157.6	39.0	15.2	0.396	11.9	4.3	38.2
3	56.6	42.4	9.5	0.379	4.5	4.9	22.8
4	56.6	40.7	10.3	0.432	3.9	4.2	19.4
5	102.5	16.5	30.0	0.380	4.0	2.5	36.5
6	102.5	16.8	30.7	0.390	3.9	2.5	37.1
7	102.5	24.0	21.6	0.540	5.1	2.4	36.5
8	102.5	22.7	23.1	0.576	4.8	2.1	32.3

In the table above, tests from 1 to 4 are from the UnB motor (SARA) and from 5 to 8 are from ULB (ULBHRE). The port diameter and fuel grain lengths, for SARA and ULBHRE respectively, are 34, 30 and 101, 107.5mm. In addition, SARA tests were conducted with 16 injectors (6 with mm and 10 with 2mm) and ULBHRE tests with, from 5 to 6, with 11 injectors (with 1.4mm) and, from 7 to 8, with 21 injectors (with 1.4mm), all of them showerhead. In [4–6] other injector types were also tested. In case of SARA motor, the algorithm was executed with the 2mm injector orifice, since it produces larger droplets (Eq. 1) and, consequently, requires a longer pre-chamber.

Running the algorithm for the 8 motors from Tab. 1, the following results were obtained:

Table 2 Results: minimum pre-chamber length required to vaporize an injected droplet

#	L_{pc}, mm (Real)	L_{pc}, mm (Simulated)	Difference, %
1	56.6	44.3	21.73 ↓
2	157.6	105.2	33.25 ↓
3	56.6	245.5	333.74 ↑
4	56.6	245.3	333.39 ↑
5	102.5	97.6	4.78 ↓
6	102.5	90.1	12.07 ↓
7	102.5	219.9	114.53 ↑
8	102.5	200.1	95.22 ↑

As it is possible to observe above, motors 1, 2, 5 and 6 could have its length decreased. However, motors 3, 4, 7 and 8 needs it to increase. It is important to mention that those results consider only the vaporization model. With the results presented in Tabs. 1 and 2, it is possible to create the stability chart, in which it is possible to compare how far, or close, the simulated motors are from the real motors. This chart is presented below:

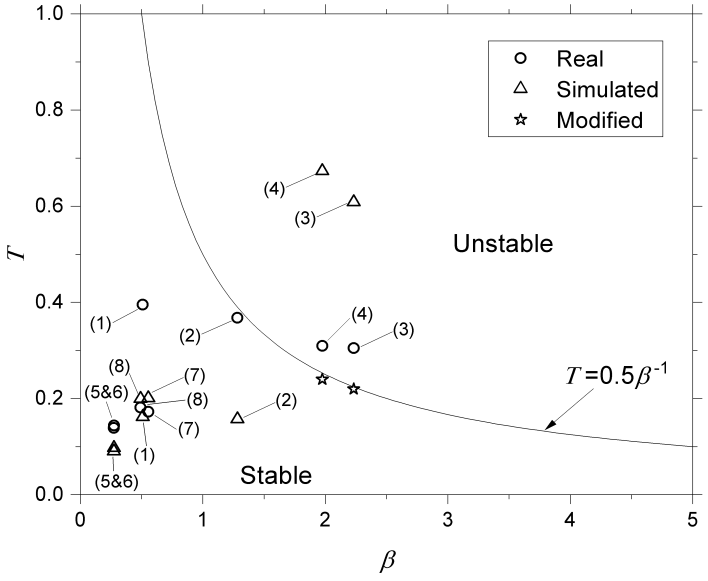

Fig. 6 Stability chart with real and simulated motors.

By analyzing all presented results, it was determined that the simulated motors, with the minimum pre-chamber length required to vaporize an injected droplet, are correspondent to all real motors (in terms of combustion stability). Since, by the vaporization analysis, it is possible to decrease L_{pc} in motors 1, 2, 5 and 6, it is shown in Fig. 6 that this reduction doesn't induce instabilities and this optimization is possible. On the other hand, motors 7 and 8 needs larger L_{pc} to complete the droplet vaporization, and this increase is possible since combustion would keep stable. However,

motors 3 and 4 would need an increase in the pre-chamber length to complete the vaporization, but it would still be unstable.

With these results, an analysis was made in order to reach a design in which the combustion would be stable for motors 3 and 4. Assuming that all other parameters are constant, this modification was easily achieved by varying the port radius. It was observed that while the port radius is increased, the required L_{pc} decreases, so as τ_{pc}. With the increase in port radius, the motor's diameter would need to increase to maintain the same burn time and the grain length would need adjustment to maintain the original thrust. This variation of τ_{pc} and L_{pc} in function of r_p is presented in the following graph:

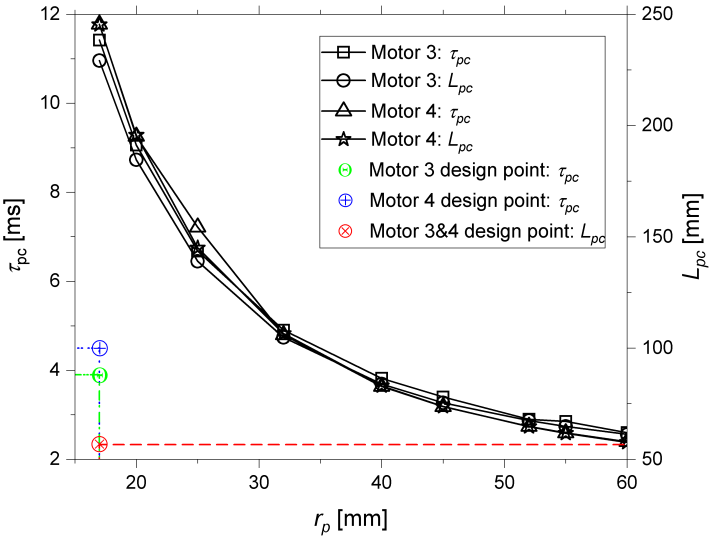

Fig. 7 Variation of τ_{pc} and L_{pc} in function of r_p.

The calculation was made by varying the port radius on an array of values.

Additionally, this analysis of the impact of r_p was extended to the other motors. It was shown that it has lower impact on combustion stability on the other cases. However, it was also possible to discuss the recommendation of using a L_{pc}/d_{pc} of 0.5 [1]. Those verification is shown below:

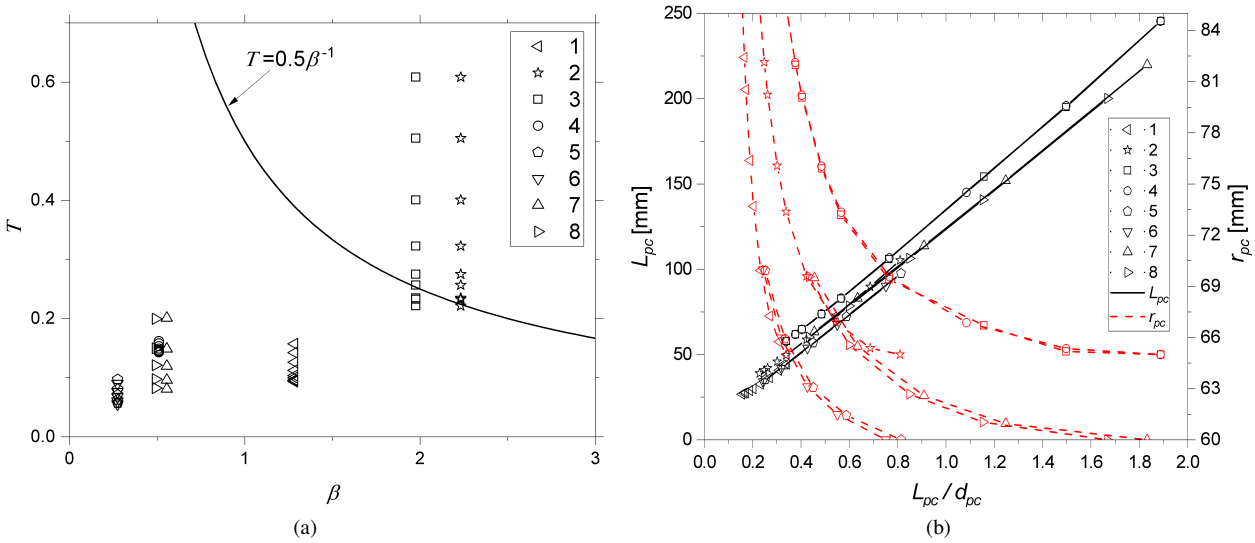

Fig. 8 Impact of r_p on (a) combustion instability and on (b) L_{pc} and L_{pc}/d_{pc}.

On Fig. 8a is shown the impact of r_p (each point for each motor is a different r_p) on $\mathcal{T}$ and how it was possible to reach stability only by varying the port radius (shown in Fig. 6). On Fig. 8b it is possible to observe that most of the values of L_{pc}/d_{pc} are concentrated between 0.25 and 0.66. In addition, the mean and median values are presented in Tab. 3. The values of r_{pc} were calculated in order to maintain the original burn times of 12s, for SARA, and 10s, for ULBHRE, and the inputs are shown in Tab. 1 and on [5, 48, 49] were used to make the internal ballistics calculations for N_2O and paraffin, considering constant oxidizer mass flow rate.

Table 3 Values of L_{pc}/d_{pc}

Parameter	Value
Mean	0.53
Median	0.38
Interval	$0.26 \leq L_{pc}/d_{pc} \geq 0.66$

The values showed in Tab. 3 were obtained excluding values from motor 3 and 4, except for the ones that make the motors stable, since they are under unstable condition. With the results presented above is valid to use the value recommended by [1]. But, since [1] suggests a range of values for the post-chamber, probably a better recommendation would be: $0.26 \leq L_{pc}/d_{pc} \geq 0.66$. However, this range should be used only on early phases of design. The ideal workflow is: use the theory presented in this work (vaporization + stability) $\Rightarrow$ CFD, for validation $\Rightarrow$ experimental verification.

The droplet vaporization results along the axial distance, or pre-chamber length, are shown below for the motor 2:

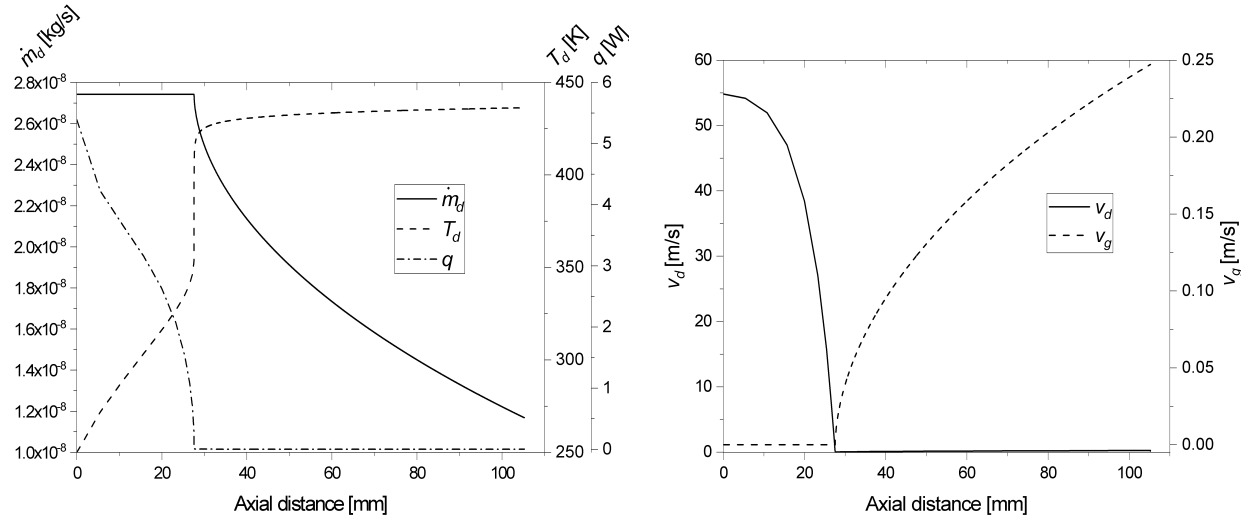

Fig. 9 Results for motor 2 of droplet vaporization of (a) $\dot{m}_d = \frac{dm}{dt}$, T_d and q, and of (b) v_d and v_g.

As it is possible to observe in Fig. 9a, the droplet is heated up until it reaches temperature required to boil the liquid, then the heat transfer is zeroed. Initially the mass flow rate variation is low because the variation of the terms in Eq. 11 are equivalent. The droplet radius and the partial pressure both increases with the increase of the temperature, but the mass transfer coefficient and the correction factor for uni-directional mass transfer both decreases, as they are inversely proportional to the the droplet radius and the partial pressure, respectively. When the vaporization begins, the droplet radius starts to decrease and so the mass flow. Also, the droplet velocity decreases significantly through the axial distance, since the droplet first expands, increasing the drag over the droplet.

Below it is shown the droplet radius histories for all motors:

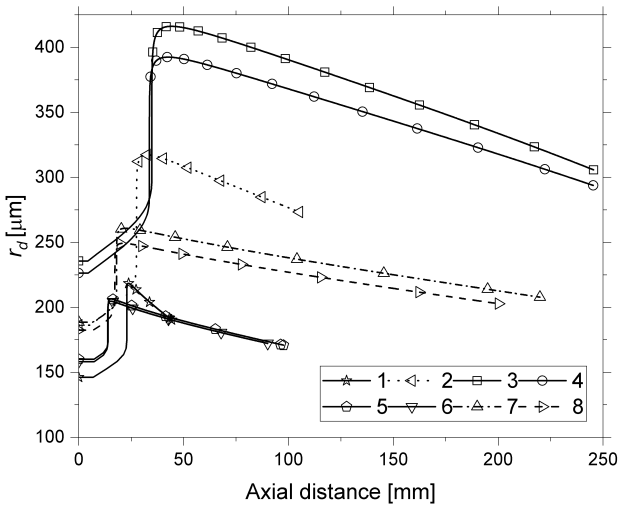

Fig. 10 Results of droplet vaporization of droplet radius with distance.

Although the droplets do not reach a diameter of zero in Fig. 10, it is shown in Fig. 9a that $\dot{m}_d$ decreases significantly and the droplet velocity reaches the final gas velocity and both reaches the port velocity ($v_d \rightarrow v_g \rightarrow v_p$), which are also convergence criteria besides the full droplet consumption (Fig. 5).

An intriguing grow in droplet radius is observed on the beginning of the axial distance. This is due to the thermal expansion and it happens because initially high molecular weight fluids expand thermally while not losing much mass by vaporization. In the case of low molecular weight fluids, the radius decrease immediately [16].

VII. Conclusions

In this work it was presented an algorithm with a vaporization model capable of optimizing pre-chambers of hybrid rocket motors, by calculating the minimum length required to vaporize an injected droplet. In addition, a verification of feed-system coupled instabilities is made. Analyzing the results, it was stated a relation between the port radius, combustion instability and the pre-chamber length. Additionally, the range of L_{pc}/d_{pc} was defined as from 0.26 to 0.66. Another characteristic of the vaporization model for the hybrids is that it only depends on the injector geometry and on the oxidizer that is being used.

The presented study is a contribution to the design of pre-combustion chambers of hybrid propellant rocket motors, which is a field of interest that has a few amount of literature references available. With this algorithm, it is possible to minimize the weight, heat transfer losses, nonuniform burn of the grain and costs with tests and suppress feed-system coupled instabilities. Future works will be conducted in order to study deeply the sensibility of each design parameter. This will allow to understand more their impact and to control and optimize the pre-chamber size more accurately. Also, this theory will be extended for the post-combustion chamber.

References

[1] Humble, R. W., Henry, G. N., and Larson, W. J., *Space Propulsion Analysis and Design*, Space Technology Series, MG-Hill, 1995.

[2] Chiaverini, M. J., and Kuo, K. K., *Fundamentals of Hybrid Rocket Combustion and Propulsion*, Reston, 2007, Vol. 218.

[3] Sutton, G. P., and Biblarz, O., *Rocket Propulsion Elements*, 2016, Vol. Ed. 9.

[4] Lee, J., Bertoldi, A. E. M., Andrianov, A., Borges, R. A., Veras, C. A. G., Battistini, S., Morita, T., and Hendrick, P., "The Role of Pre-Combustion Chamber Design in the Feed-System Coupled Instability of Hybrid Rocket," *Journal of Propulsion and Power, 36 (6), 796-805*, 2020.

[5] Bertoldi, A. E. M., "Study of Combustion Instability in Hybrid Propellant Rocket Motor (in portuguese)," *Doctorate thesis, University of Brasília, Department of Mechanical Engineering*, July 2018.

[6] Bertoldi, A. E. M., Bouziane, M., Lee, J., Veras, C. A. G., Hendrick, P., and Simone, D., "Theoretical and Experimental Study of Combustion Instability in Hybrid Rocket Motors," *8^t h European Conference for Aeronautics and Space Sciences*, 2019.

[7] Sporschill, G., "Numerical approach of a hybrid rocket engine behaviour - Modelling the liquid oxidizer injection using a Lagrangian solver," *Masters Dissertation in Aerospace Engineering, Multi-Physics for Energetics Department, ENSTA*, 2017.

[8] F, S. C., and Vieira, R., "Preliminary Analysis of Hybrid Rockets for Lauchung Nanosats into LEO," *Journal of the Brazilian Society of Mechanical Science and Engineering, Vol. 32, No. 4*, 2010.

[9] Gamper, E., and Hink, R., "Design and Test of Nitrous Oxide Injectors for a Hybrid Rocket Engine," *Deutscher Luft-und Raumfahrtkongress*, 2013.

[10] Gontijo, M. S., "A Review of Vaporization Models as Design Criterion for Bipropellant Thrust Chambers," *Aerospace Technic and Technology*, 2022.

[11] Turns, S. R., *An Introduction to Combustion: Concepts and Applications*, 2011, Vol. Ed. 3.

[12] Priem, R. J., and Heidmann, M. F., "Vaporization of Propellants in Rocket Engines," *ARS Journal, 29, 836-842*, 1959.

[13] Priem, R. J., "Propellant Vaporization as a Criterion for Rocket Engine Design; Calculations of Chamber Length to Vaporize a Single n-Heptane Drop," *NACA - National Advisory Committee for Aeronautics, Technical Note 3985*, 1957.

[14] Priem, R. J., "Propellant Vaporization as a Criterion for Rocket Engine Design; Calculations Using Various Log-Probability Distributions of Heptane Drops," *NACA - National Advisory Committee for Aeronautics, Technical Note 4098*, 1957.

[15] Priem, R. J., "Propellant Vaporization as a Criterion for Rocket Engine Design; Calculations of Chamber Length to Vaporize Various Propellants," *NACA - National Advisory Committee for Aeronautics, Technical Note 3883*, 1958.

[16] Priem, R. J., Borman, G. L., Walkil, M. M. E., Uyehara, O. A., and Myers, P. S., "Experimental and Calculated Histories of Vaporizing Fuel Drops," *NACA - National Advisory Committee for Aeronautics, Technical Note 3988*, 1957.

[17] Spalding, D. B., "Combustion in Liquid-Fuel Rocket Motors," *Imperial College of Science and Technology, London*, 1958.

[18] Spalding, D. B., "A One-Dimensional Theory of Liquid-Fuel Rocket Combustion," *Imperial College of Science and Technology, London*, 1959.

[19] Adler, J., "A One-Dimensional Theory of Liquid-Fuel Rocket Combustion. Part II. The Influence of Chemical Reaction," *Imperial College of Science and Technology, London*, 1959.

[20] Khan, T., Qamar, I., Shah, F., Akhtar, K., and Akhtar, R., "Model for Fuel Droplet Evaporation in Combustion Chamber of Liquid Propellant Rocket Engines," *Journal of Engineering and Applied Sciences, Vol. 37, No. 1*, 2018.

[21] Khan, T., and Qamar, I., "Factors Affecting Characteristic Length of the Combustion Chamber of Liquid Propellant Rocket Engines," *Mehran University Research Journal of Engineering and Technology, Vol. 38, No. 3*, 2019.

[22] Salvador, C. A. V., "Mathematical Model of Bipropellant Combustion Chambers (in portuguese)," *Masters dissertation on Space Engineering and Technology/Combustion and Propulsion - INPE*, 2004.

[23] Wang, Z. G., "Internal Combustion Process of Liquid Rocket Engines: Modeling and Numerical Simulations," *Wiley*, 2016.

[24] Belal, H. M., "Numerical Simulation of Spray Combustion," *Master dissertation on Military Technical College (MTC)*, 2010.

[25] Belal, H. M., "Validation of a Simplified Model for Liquid Propellant Rocket Engine Combustion Chamber Design," *IOP Conference Series Materials Science and Engineering*, 2020.

[26] Belal, H. M., "Vaporization-Controlled Simplified Model for Liquid Propellant Rocket Engine Combustion Chamber Design," *IOP Conference Series Materials Science and Engineering*, 2019.

[27] Gontijo, M. S., Fischer, G. A. A., and Costa, F. S., "Evaluation of SMD Effects on Characteristic Lengths of Liquid Rocket Engines Using Ethanol/LOx and RP-1/LOx," 18^{th} *Brazilian Congress of Thermal Sciences and Engineering*, 2020.

[28] Gontijo, M. S., Fischer, G. A. A., and Costa, F. S., "Influence of SMD on Characteristic Lengths of Liquid Propellant Rocket Eengines," 8^{th} *School of Combustion*, 2021.

[29] Gontijo, M. S., Fischer, G. A. A., and Costa, F. S., "Characteristic Lengths of Liquid Propellant Rocket Engines and the Influence of Chemical Reactions," 26^{th} *International Congress of Mechanical Engineering*, 2021.

[30] Karabeyoglu, A., Dyer, J., Stevens, J., and Cantwell, B., "Modeling of N_2O Decomposition Events," *44th AIAA/ASME/SAE/ASEE Joint Propulsion Conference Exhibit*, 2008.

[31] Lefebvre, A. H., and McDonell, V. G., "Atomization and Sprays," *CRC Press, 2ª Ed.*, 2007.

[32] Saeedipour, M., Schneiderbauer, S., Pirker, S., and Bozorgi, S., "A Numerical and Experimental Study of Flow Behavior in High Pressure Die Casting," *Magnesium Technology, 185-190*, 2014.

[33] Schimdt, P. W., "Zerstäuben von Flüssigkeiten," *Physik in Unserer Zeit, 113-120*, 1984.

[34] Shynkarenko, O., and Gontijo, M. S., "Investigation of a Dual-Fuel Hybrid Rocket Engine for Missile and Rocket Applications," 71*st International Astronautical Congress (IAC) - The CyberSpace Edition*, 2020.

[35] Waxman, B. S., "An Investigation of Injectors for use with High Vapor Pressure Propellants with Applications to Hybrid Rockets," *Doctorate thesis on the Department of Aeronautics and Astronautics of the Stanford University*, 2014.

[36] Nurick, W. H., "Orifice Cavitation and Its Effect on Spray Mixing," *Journal of Fluids Engineering, 98(4), 681*, 1976.

[37] Whitmore, S. A., and Chandler, S. N., "Engineering Model for Self-Pressurizing Saturated-N_2O-Propellant Feed Systems," *Journal of Propulsion and Power, Vol. 26, No. 4, July-August*, 2010.

[38] Dyer, J., Doran, E., Dunn, Z., Lohner, K., Zilliac, G., and Cantwell, B., "Modeling Feed System Flow Physics for Self-Pressurizing Propellants," *43rd AIAA/ASME/SAE/ASEE Joint Propulsion Conference Exhibit, July*, 2007.

[39] Solomon, B. J., "Engineering Model to Calculate Mass Flow Rate of a Two-Phase Saturated Fluid Through An Injector Orifice," *Master dissertation on the Department of Mechanical and Aerospace Engineering of the Utah State University*, 2011.

[40] Linstrom, P. J., "A Guide to the NIST Chemistry WebBook," *National Institute of Standards and Technology (NIST)*, 2022.

[41] Zimmerman, J. E., Waxman, B. S., Cantwell, B. J., and Zilliac, G. G., "Review and Evaluation of Models for Self-Pressurizing Propellant Tank Dynamics," *49th AIAA/ASME/SAE/ASEE Joint Propulsion Conference*, 2013.

[42] Zilliac, G., and Karabeyoglu, M. A., "Modeling of Propellant Tank Pressurization," *41st AIAA/ASME/SAE/ASEE Joint Propulsion Conference*, 2005.

[43] Filho, R. B. N., and Gontijo, M. S., "Performance Prediction Software for Hybrid Rocket Motors," *18th Brazilian Congress of Thermal Sciences and Engineering*, 2020.

[44] Gontijo, M. S., and Filho, R. B. N., "Two-Phase Tank Emptying and Burnback Coupled Internal Ballistics Prediction on Hybrid Rocket Motors," *Workshop in Space Engineering and Technologies*, 2020.

[45] Gontijo, M. S., and Filho, R. B. N., *Two-Phase Tank Emptying and Burnback Coupled Internal Ballistics Prediction on Hybrid Rocket Motors*, 3rd ed., Atena Editora, Paraná, 2021, Chap. 5.

[46] Niño, E. V., and Razavi, M. R., "Design of Two-Phase Injectors Using Analytical and Numerical Methods with Application to Hybrid Rockets," *AIAA Propulsion and Energy Forum*, 2019.

[47] Summerfield, M. A., "A Theory of Unstable Combustion in Liquid Propellant Rocket Systems," *Journal of the American Rocket Society, vol. 21, no. 5. 6 p.*, 1951.

[48] Andrianov, A., Shynkarenko, O., Bertoldi, A. E. M., Barcelos, M. N. D. J., and Veras, C. A. G., "Concept and Design of the Hybrid Test-Motor for Development of a Propulsive Decelerator of SARA Reentry Capsule," *51st AIAA/SAE/ASEE Joint Propulsion Conference, AIAA Paper 2015-3941*, 2015.

[49] Bouziane, M., Bertoldi, A. E. M., Lee, D., Milova, P., Hendrick, P., and Lefebvre, M., "Design and Experimental Evaluation of Liquid Oxidizer Injection System for Hybrid Rocket Motors," *7^{th} European Conference for Aeronautics and Space Sciences*, 2017.

[50] Karabeyoglu, A. M., Zilwa, S., Cantwell, B., and Zilliac, G., "Modeling of Hybrid Rocket Low Frequency Instabilities," *Journal of Propulsion and Power, Vol. 21, No. 6, November–December*, 2005.

[51] Sirignano, W. A., *Fluid Dynamics and Transport of Droplets and Sprays*, 201, Vol. Ed. 2.

[52] Ranz, W. E., and Marshall, W. R., "Evaporation From Drops," *Chemical Engineering Progress, Vol. 48, No. 3, 141-146*, 1952.

[53] Ingebo, R. D., "Vaporization Rates and Drag Coefficients for Isooctane Sprays in Turbulent Air Streams," *NACA - National Advisory Committee for Aeronautics, Technical Note 3265*, 1954.

[54] Abramzon, B., and Sirignano, W. A., "Droplet Vaporization Model for Spray Combustion Calculations," *International Journal of Heat Mass Transfer, Vol. 32n No. 9, 1605-1618*, 1989.